Multi-quadrupole scan for emittance determination at PITZ

Susan Skelton

University of St Andrews, Scotland
Email: ses12@st-andrews.ac.uk

DESY Zeuthen

PITZ is a test facility for the development of high quality electron sources. One of the most important beam characteristics is transversal emittance. This work investigates the use of multi-quadrupole scan technique for emittance measurement. Experimental results for both single and multi-quadrupole scans are presented. Simulations were performed and the results are shown for comparison with experimental results. Finally, suggestions for further investigations for the development of the multi-quadrupole scan technique are overviewed.

CONTENTS

1. INTRODUCTION

The acronym PITZ stands for Photo Injector Test Facility at DESY Zeuthen. As the name suggests it is a dedicated test facility for research and development of laser driven electron sources for Free Electron Lasers and Linear Colliders. Previous accomplishments include the electron gun for FLASH (Free electron LASer in Hamburg). X-ray Free Electron Lasers (XFELs), such as European XFEL project, require a beam of even higher quality. The work currently in progress is involved with optimising the electron source for these applications.

1.1 Free electron lasers

Free electron lasers (FELs) produce extremely highly brilliant, coherent electromagnetic radiation with a short wavelength. This electromagnetic radiation is generated by the acceleration of charged relativistic particles in the presence of magnetic fields. In a FEL, the radiation is produced by rapidly applying alternating accelerating and decelerating forces on the electrons in the plane perpendicular to their propagation direction. This is achieved by passing the beam through a periodic magnet called an undulator. The electrons assume a sinusoidal path and emit radiation due to their deceleration. The quality of the radiation beam produced is limited ultimately by the quality of the electron beam with which it was formed; hence the development of high quality electron beams is crucial.

Radiation produced in FELs has a number of desirable properties. Most importantly, it has a very high brightness, of the order of hundreds of thousands of times brighter than that from a conventional X-ray tube. The radiation is highly polarised and is emitted in pulses less than 1ns, giving extremely high peak power. If the energies of the particles and magnetic fields are large enough, the wavelength of the radiation can be of the order of X-rays. FELs have applications in a wide range of areas including medicine, molecular biology and crystallography [1].

1.3 PITZ set-up

The PITZ set-up consists of a 1.5 cell normal conducting RF gun with Cs_2Te photocathode and its laser system, two solenoid magnets, a normal conducting booster cavity, and diagnostic systems upstream and downstream of the booster cavity. The RF gun and the booster cavity are operated with separated L-band (1.3 GHz) RF power systems. The schematic layout of PITZ is shown in Fig. 1.
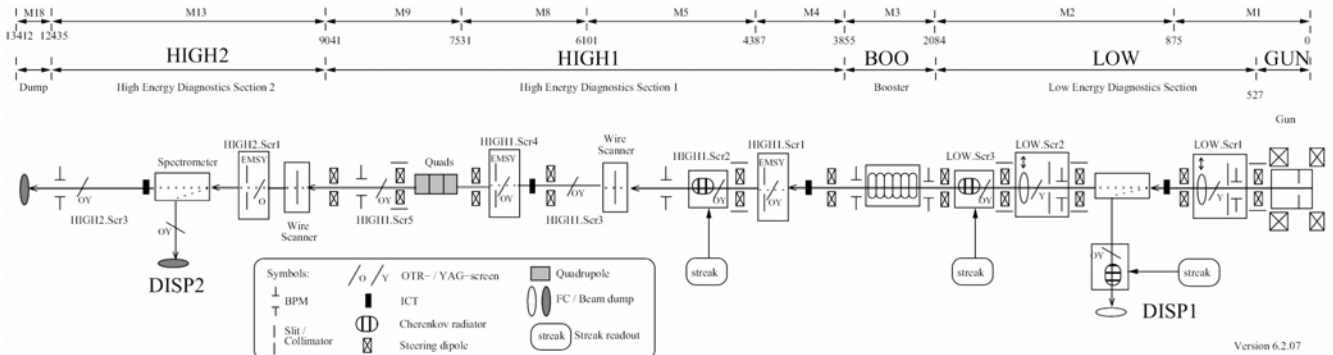
Fig 1. Schematic layout of the PITZ beam line.

The laser system at PITZ is a frequency quadrupled Nd:YLF laser which produces UV pulses at a wavelength of 262 nm with pulse length of about 20 ps and a separation of 1 μs. When the laser beam is incident on the Cs_2Te cathode surface, electrons are emitted and are accelerated due to a time-varying electromagnetic field inside a standing wave RF gun, resulting in electron beams with energies depending on the input RF power level. Currently, the maximum energy gain from the RF gun at PITZ is around 6.5 MeV. An electron beam is focused by the magnetic field from the main solenoid magnet. A so-called bucking magnet compensates for

the magnetic field at the cathode reducing the residual angular momentum of the electrons. Downstream of the RF gun, the booster cavity is placed for post acceleration and accelerates electrons up to ~15 MeV [2].

The beam diagnostic section includes extensive devices enabling a comprehensive study of beam parameters. Faraday cups and integrating current transformers (ICTs) measure the beam charge. The beam size, beam shape and position can be measured using YAG or OTR view screen stations with CCD cameras or using wire scanners. Three emittance measuring systems (EMSYs) using the slit scan method measure the transverse emittance. Streak cameras allow the longitudinal bunch parameters to be investigated. Two dipole spectrometers allow the momentum and momentum spread of the particles to be determined both before and after the booster cavity [3]. Quadrupole magnets are planned to be used for both phase space tomography and emittance measurement. This work focussed on the latter case.

2. BASIC BEAM DYNAMICS CONCEPTS

2.1 Beam Ellipse
A beam of N particles can be described by a set of N points in the 6 dimensional phase space, $\{x, y, z, p_x, p_y, p_z\}$. Neglecting any coupling forces, this phase space can be split into two 2-dimensional transverse phase spaces $\{x, p_x\}$, $\{y, p_y\}$, and one longitudinal phase space $\{z, p_z\}$. The particles of interest in the phase space distribution can be considered to be bounded by an ellipse in phase space. This ellipse is defined by a symmetric, positive-definite matrix called the beam matrix, $\sigma(z)$ [6];

$$\sigma(z) = \begin{bmatrix} \sigma_{11}(z) & \sigma_{12}(z) \\ \sigma_{12}(z) & \sigma_{22}(z) \end{bmatrix} \tag{1}$$

Physical components of the beam matrix are illustrated in Fig. 2. As the beam propagates, the shape and orientation of the beam ellipse changes but the ellipse area is invariant along propagation as assured by Liouville's theorem in Hamiltonian mechanics: "the phase-space distribution function is constant along the trajectories of a system". Therefore this ellipse area is a very useful parameter for characterising the beam.

2.2 Emittance
The emittance is a figure of merit used to characterise and compare the quality of different beams. There are a number of alternate definitions but they are all functions of the beam ellipse area.

$$x'_{max} = \sqrt{\sigma_{22}}$$

$$\tan 2\varphi = \frac{2\sigma_{12}}{\sigma_{22} - \sigma_{11}}$$

$$x_{max} = \sqrt{\sigma_{11}}$$
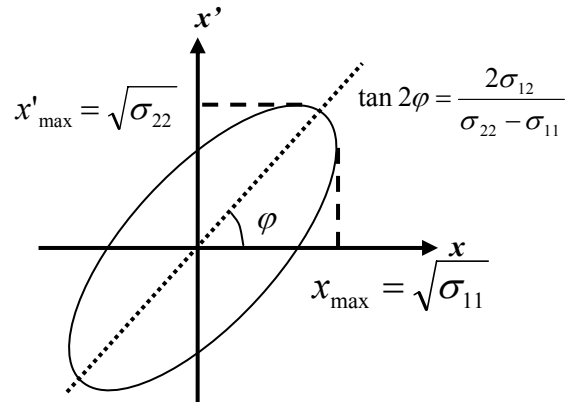
Fig 2. The beam ellipse and physical interpretation of the beam matrix compnonents.

Assuming that the distribution is bounded by an ellipse as described above, the emittance, ε, can be expressed as

$$\varepsilon = Area = \pi \sqrt{\det \sigma} \tag{2}$$

The quoted emittance is usually normalised with the beam energy in order to compare the beams' quality independently of acceleration effect. Hence, the normalised emittance becomes

$$\varepsilon_n = \beta\gamma \sqrt{\det \sigma} \tag{3}$$

where β and γ are the relativistic factors

$$\beta = \frac{v}{c} \text{ and } \gamma = \frac{1}{\sqrt{1 - \beta^2}}$$

3

However, the shape of the phase space area can be distorted due to space charge forces or nonlinear forces in the focussing systems. Then the transverse beam properties differ from the above definition, hence the emittance should not be conserved.

An alternative definition of the emittance, the **root mean square (rms) emittance**, gives a more complete description [4]. In this case, the moments of the particle distribution in transverse phase space are used and the moments are related to the beam matrix elements as:

$$\sigma_{11} = \langle x^2 \rangle = \int\int dxdx' f_2(x,x')x^2$$
$$\sigma_{12} = \langle xx' \rangle = \int\int dxdx' f_2(x,x')xx' \tag{4}$$
$$\sigma_{22} = \langle x'^2 \rangle = \int\int dxdx' f_2(x,x')x'^2 .$$

The beam matrix components have the following interpretations. The first component (σ_{11}) is the square of the rms size of the beam, the second component (σ_{12}) is the cross correlation term and the final component (σ_{22}) is the square of the beam divergence. Therefore, the normalised rms emittance can be expressed simply as

$$\varepsilon_{n,rms} = \beta\gamma\sqrt{\langle x^2 \rangle\langle x'^2 \rangle - \langle xx' \rangle^2} . \tag{5}$$

In principle, the normalised rms emittance is conserved along the beam line. In practice, however, space charge forces and some non-linear electromagnetic forces cause it to increase.

The **space-charge** force is the repulsive Coulomb force due to the high density of charged particles in the bunch. This distorts the phase space ellipse, increasing the rms emittance as shown in Fig 3. Accelerating the beam to higher energies reduces the ratio of transverse to longitudinal velocities, hence the divergence, thus reducing the growth of emittance due to space-charge forces.

(a)   (b)
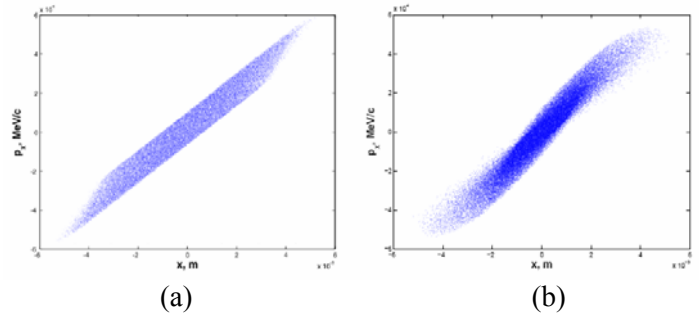
Fig. 3. ASTRA simulations illustrating the phase space distortion due to space charge forces [2]. The plots show the phase space distribution not including (a) and including (b) space charge interactions.

2.3 Matrix Formalism

The motion of particles in the beam can be described by a system of coupled, second order, inhomogeneous differential equations. The solutions to these equations determine the components in matrices called transformation matrices [5]. The beam matrix at some distance z is related to the beam matrix at z_0 by

$$\sigma(z) = R(z)\sigma(z_0)R^T(z) \tag{6}$$

where R(z) is the transformation matrix from z_0 to z. The matrices $\sigma(z_0)$ and $\sigma(z)$ are the beam matrices in Eq. (1), with the components defined as shown in eq'n (4), with $x = z_0$ or z. Thus if the transformation matrices of all components are known, it is possible to describe the trajectory of the beam along the beam transport line.

3. QUADRUPOLE SCAN TECHNIQUE

3.1 Quadrupole magnet and transformation matrices
A quadrupole magnet consists of four iron pole shoes with hyperbolic contour producing magnet field as shown in Fig 4. In the magnetic field of the quadrupole magnet, the transverse motions in the x and y planes uncouple, thus two linearly independent solutions exist to the differential equation and matrices can be found to describe each plane separately [4].
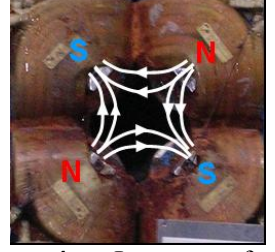
Fig 4. Image of a quadrupole magnet with the field lines superposed.

The magnetic field of a quadrupole magnet is linear in the deviation from the axis with

$$B_x = -g \cdot y \text{ and } B_y = -g \cdot x \tag{7}$$

where g is the gradient of the magnetic field. The resultant forces are focussing in one transverse plane and defocusing in the other, depending on the relative direction between particle velocity and magnetic field, and on the sign of the charge of the particles. The transformation matrices [6] describing the evolution of the beam through the quadrupoles are

$$R_Q(focus) = \begin{bmatrix} \cos\phi & \frac{1}{\sqrt{k}}\sin\phi \\ -\sqrt{k}\sin\phi & \cos\phi \end{bmatrix} \tag{8}$$

and

$$R_Q(defocus) = \begin{bmatrix} \cosh\phi & \frac{1}{\sqrt{|k|}}\sinh\phi \\ \sqrt{|k|}\sinh\phi & \cosh\phi \end{bmatrix} \tag{9}$$

where the phase angle is

$$\phi = \sqrt{k}\, l_{eff} \tag{10}$$

and k is the focussing strength of the quadrupole which is given by [6]

$$k = 0.2998 \frac{g[T/m]}{p[GeV]}. \tag{11}$$

The effective length (l_{eff}) is defined by

$$l_{eff} = \frac{\int g(z)dz}{g_{max}} \tag{12}$$

where g_{max} is the gradient of the magnetic field at the pole tip.

In the transformation matrix model described above, the quadrupole magnets are assumed to have constant field strength over their effective length, and zero field strength elsewhere. This is the so called hard-edge model. In the drift space region, there is no existing force and the transformation matrix is represented by

$$R_d = \begin{bmatrix} 1 & d \\ 0 & 1 \end{bmatrix} \tag{13}$$

where d is the length of drift space. To obtain the transformation matrix for the whole path, the sequence of incremental matrices must be multiplied together.

3.2 Quadrupole scan technique

If the transformation matrix of the whole path of beam transportation is known, the beam matrix components in Eq. (4) can be defined and hence the emittance can be calculated. Utilising the correlation between beam size and quadrupole magnetic field in the transformation matrix model, the emittance value can be obtained. This method is well known as the "quadrupole scan technique". In the quadrupole scan technique, Eq. (6) is paramount. Quadrupole magnets with known transformation matrices are used, thus from measurements of the beam size at a distance z after the magnets, the beam matrix at z_0 can be calculated.

Let R be the total transformation matrix for the system of quadrupoles and drift spaces from distance z_0 to z:

$$R = \begin{bmatrix} R_{11} & R_{12} \\ R_{21} & R_{22} \end{bmatrix}. \tag{14}$$

Thus from Eq. (6), the first term in the resultant matrix is

$$\sigma_{11}(z) = \sigma_{11}(z_0)R_{11}^2 + 2\sigma_{12}(z_o)R_{11}R_{12} + \sigma_{22}(z_0)R_{12}^2 = f(g). \tag{15}$$

A quadrupole scan consists of a set of N beam size measurements at a fixed distance from the quadrupole magnet, as the quadrupole field strength is scanned over a range of values. This produces a distribution as, for example, shown for a single quadrupole scan in Fig. 5. The coefficients of the beam matrix $\sigma(z_0)$ are determined by minimising Eq. (16).

$$\sum_i^N \left(\sigma_{11_i} - f(g_i) \right) \tag{16}$$

The emittance is then calculated using Eq. (3).

The quantity $\sqrt{\sigma_{11}}$ is the measured rms beam size after the quadrupole system. The parameter g is the gradient in the quadrupole magnet.

The basic single quadrupole scan technique is a well established method of emittance determination [6]. However, for some quadrupole gradients around the focus the beam is very small and the particle density is comparatively high, thus the effects of space charge are larger. Space charge is more difficult to account for in the matrix method, so it is desirable to modify the method to minimise space charge effects by using a multi quadrupole system to maintain a large beam size at the focus due to interplay between focussing and defocusing magnets.

Fig 5. Typical distribution from ASTRA simulation of beam sizes, as measured at some distance z after the single quadrupole magnet, as a function of quadrupole field gradient.

In our consideration, a quadrupole triplet is used. The quadrupole triplet at PITZ consists of three magnets, of which the first and third are identical, each separated by a drift space of length d. For the triplet quadrupole scan, function f(g) becomes f(g_1, g_2) where g_1 is the magnetic field gradient of quadrupoles 1 and 3 (corresponding to current I_1 in Fig. 6), and g_2 is the magnetic field gradient of quadrupole 2 (corresponding to current I_2 in Fig. 6).

For triplet-quadrupole scan, it is useful to find the optimum data points to take to reconstruct the rms size surface for emittance determination as shown in Fig. 6. There are three types of possible scan: 1) scan across the minimum of the surface varying the field gradient of either quadrupoles 1 and 3, or only 2, but keeping the others constant; 2) scan across the minimum of the surface varying the field gradient of all quadrupoles; 3) scan across some local minimum but not across the global minimum, thus maintaining larger beam sizes. It is necessary to investigate how the emittance calculation depends on which regime is followed.
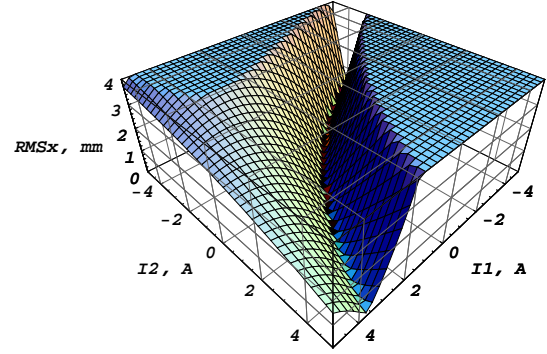
Fig. 6. Rms size surface for triplet-quadscan. I_1 is the current in Q_1 and Q_3, and I_2 is the current in Q_2.

4. EXPERIMENT

4.1 Experimental set-up
The quadrupole arrangement used in the PITZ beam line is situated at z=7.851m (entrance) and has parameters as indicated in Table 1 and Fig. 7. The first (Q_1) and third (Q_3) magnets are identical and have the same current supply, but the second (Q_2) has double the length and opposite field direction.

Parameter	Quadrupoles 1, 3	Quadrupole 2
Geometrical length	60 mm	120 mm
Effective length	77 mm	139 mm
Geometrical drift space between quadrupoles	80 mm	
Effective drift space between quadrupoles	62 mm	
Bore radius	20 mm	20 mm
Maximum current	5 A	5 A
Gradient at I=5A	2.55 T/m	2.55 T/m

Table 1. Parameters of the Triplet Quadrupole Magnets used in the experiments.
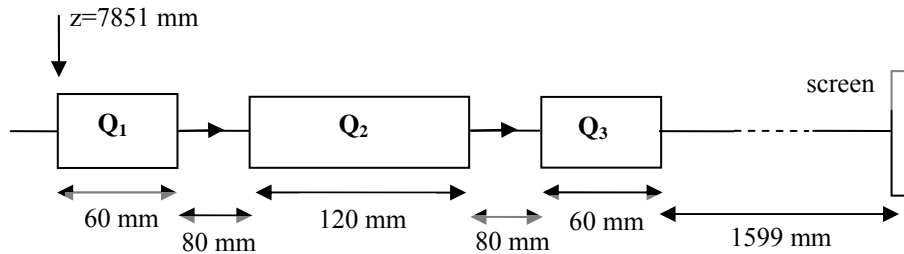
Fig. 7. Schematic depiction of the Triplet Quadrupole Magnets used in the experiments.

4.2 Experimental Procedure
To begin with, the equipment had to be set up to provide a suitable beam for the experiment. Firstly, a suitable laser profile was obtained. The nominal longitudinal profile was a flat top pulse with ~20 ps FWHM and ~ 6-7 ps rise/fall time. The transverse laser rms size ranged from ~ 0.3 - 0.6 mm. Next, the optimum phase of the rf gun was determined so as to give maximum mean momentum which is about 6.4 MeV/c. The bunch charge was measured. A phase scan of the booster cavity was performed to determine the optimum phase for maximum acceleration and the energy after the booster cavity was measured. Further, the solenoid field was scanned over a range which produces the minimum rms size at a certain z position. Screens chosen for this scan were High1.Scr1. (z=4.287m). and High2.Scr1. (z=9.850m). The optimised beam was then aligned

through the quadrupoles onto the observation screen being used for measurements (either High1.Scr5. or High2.Scr1.). The region of measurement was determined by varying quadrupole fields and observing the location of the minimum rms beam size. Finally, both single (to develop the method and enable comparison) and multi- quadscans were performed. The emittance was calculated using the algorithm described in section 3.2.

4.3 Results and Discussion

The calculated values of emittance from the measurements are presented in Tables 2 and 3 with the measured minimum emittance from single slit scan method at High1.Scr1. (or EMSY1) screen [7]. ε_x and ε_y are the emittances in the x and y planes respectively, and ε is the geometrical average. The errors quoted are statistical errors. I_{main} is the main solenoid current. X pos. jitter and Y pos. jitter are the standard deviation from the mean position values on the screen in x and y planes for different quadrupole field strengths.

#	E (MeV)	Charge (nC)	I_{main} (A)	Measured with quads					Measured at EMSY		
				ε_x (mm mrad)	ε_y (mm mrad)	ε (mm mrad)	X pos. jitter (mm)	Y pos. jitter (mm)	ε_x (mm mrad)	ε_y (mm mrad)	ε (mm mrad)
1	12.94	1.002	350	2.50±0.41	2.06±0.13	2.27±0.24	1.47	0.08	2.88	2.20	2.59
2	12.94	1.002	370	2.49±0.24	1.88±0.18	2.16±0.20	1.77	0.29	2.88	2.20	2.59
3	10.46	0.005	190	0.75±0.05	1.7±0.14	1.13±0.13	0.72	0.20	0.50	0.47	0.49
4	10.49	1.003	352	2.14±0.05	1.29±0.5	1.66±0.34	0.66	0.59	0.83	1.06	0.94
5	10.47	1.009	352	2.63±0.08	3.86±0.1	3.19±0.23	0.84	1.52	1.25	1.26	1.26

Table 2. Comparison of experimental results for single quadscans at the entrance of quadrupole (*z*=7.851 m) and measured emittance values at EMSY1 (*z*=4.287 m).

#	E (MeV)	Charge (nC)	I_{main} (A)	Measured with quads					Measured at EMSY		
				ε_x (mm mrad)	ε_y (mm mrad)	ε (mm mrad)	X pos. jitter (mm)	Y pos. jitter (mm)	ε_x (mm mrad)	ε_y (mm mrad)	ε (mm mrad)
6	9.51	0.199	335	0.65±0.27	-	-	0.98	0.81	-	-	-
7	13.03	0.193	340	3.35±0.05	2.60±0.02	2.95±0.03	1.98	0.41	0.92	1.05	0.98
8	14.47	1.009	352	3.17±0.08	4.92±0.09	3.95±0.09	1.28	1.28	1.25	1.26	1.26
9	14.47	1.009	352	2.55±0.07	3.41±0.05	2.95±0.06	1.50	0.58	1.25	1.26	1.26
10	14.47	1.009	370	4.96±0.45	2.18±0.08	3.29±0.21	0.13	0.49	1.25	1.26	1.26
11	14.47	1.009	352	1.86±1.08	2.23±0.23	2.04±0.69	0.99	0.78	1.25	1.26	1.26

Table 3. Comparison of experimental results for multi-quadscans at the entrance of quadrupole (*z*=7.851 m) and measured emittance values at EMSY1 (*z*=4.287 m).

The emittance values measured using the quadrupole scan method differ from those measured at EMSY1 using the single slit scan method. This is mainly due to the fact that the measured emittance is dependent on the solenoid field and varies along the beam line. During experiments, the beam was focussed either at High2.Scr1. or at EMSY1, and not at the quadrupole entrance. Hence the emittance measured at the quadrupole entrance is greater than that at EMSY1 (High1.Scr1.). Secondly, the simple approximation used to describe the field in the quadrupoles in the algorithm is too far from the physical field distribution. For better accuracy, magnetic field fringe effects should be considered.

It is important to note here that it was not possible to fit the data for quadscans which did not cross the global minimum of the rms size surface. More theoretical study is required in this area. It is also necessary to develop some criteria for beam alignment through the quadrupole magnets.

5. SIMULATIONS

5.1 Procedure

Beam dynamic simulations were performed using the code ASTRA (A Space Charge Tracking Algorithm) [8] to compare with experimental results. All the main beam line components were included and were matched to the corresponding values used in the experiments, i.e. longitudinal and transverse laser beam profiles, bunch charge, field gradient for rf gun and booster cavities, magnetic field for solenoid magnets and field gradient for quadrupole magnets.

Scans of the main solenoid field producing different rms beam sizes were performed at various distances along the beam line in order to enable comparison with experimental results. Quadrupole scans were also simulated and the resultant data was fitted using the same algorithm as for the experiments.

5.2 Results and Discussion

5.2.1 Solenoid scan

The main solenoid field was scanned for various locations matched to experimental locations; EMSY1 screen (z=4.3 m), entrance to quadrupole magnets (z=7.8 m), High1.Scr5. (z=8.6 m) and High2.Scr1. (z=9.85 m). The simulation results (see Fig. 8) show that the minimum emittance is around the point of minimum rms beam size. Therefore, the main solenoid current was chosen to be that which produces minimum rms size at the chosen z position. The difference between the solenoid field producing minimum rms size and the field producing minimum emittance was 2.954×10^{-4} T or 0.13% of the focussing field.
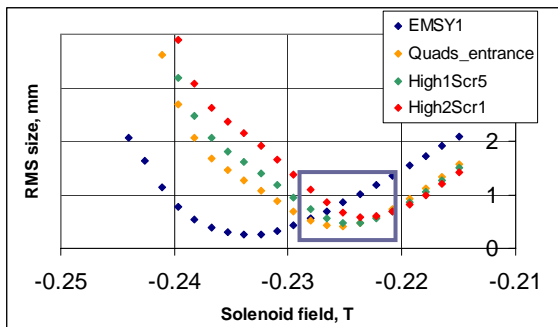
(a) RMS beam size as a function of main solenoid field
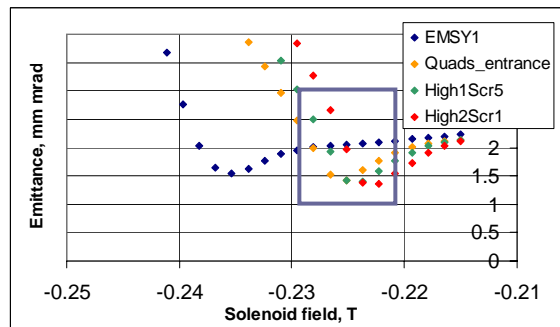
(b) Beam emittance as a function of main solenoid field
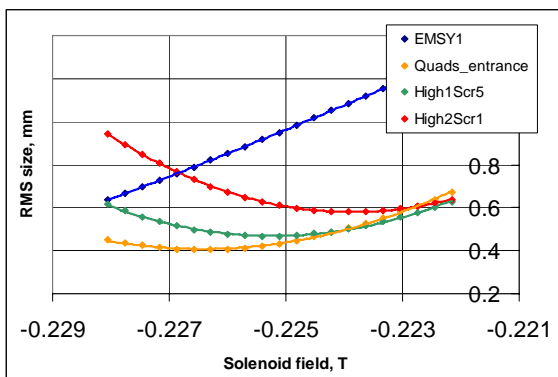
(c) Enlarged selected area marked in 6(a) above
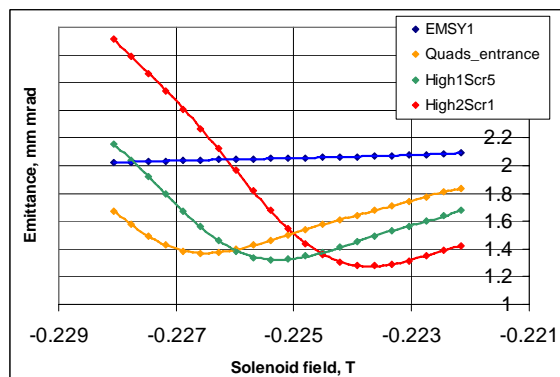
(d) Enlarged selected area marked in 6(b) above

Fig. 8. Results of the ASTRA simulations for the main solenoid scan. Emittances at the quadrupole entrance when beam is focussed at EMSY1 screen and at High2.Scr1. are 3.85 mm mrad and 1.64 mm mrad, respectively.

9

In ASTRA simulations, when the beam was focussed at the entrance to the quadrupole magnets, the minimum emittance was 1.36 mm mrad. However, in the experiments, it was not possible to observe the beam at the entrance to the quadrupole magnets due to the lack of a screen at that location. The beam was focussed either at High1.Scr1. (EMSY1) or at High2.Scr1. The simulation results in Fig. 8(d) show that the emittance calculated using this method is greater than the minimum value and the difference in emittance values when the beam is focussed at EMSY1 and High2.Scr1. are +0.7 mm mrad and +0.3 mm mrad, respectively. To match the experimental results, it is necessary to have an observation screen at the quadrupole entrance for the solenoid scan.

The evolution of the rms beam size and the beam emittance along the propagation direction for solenoid fields focussing at EMSY1 and High2.Scr1. were plotted in Fig. 9 to show the influence of the focussing distance on these quantities. For large focussing distances, the emittance is smaller at the distance of the quadrupole magnets.
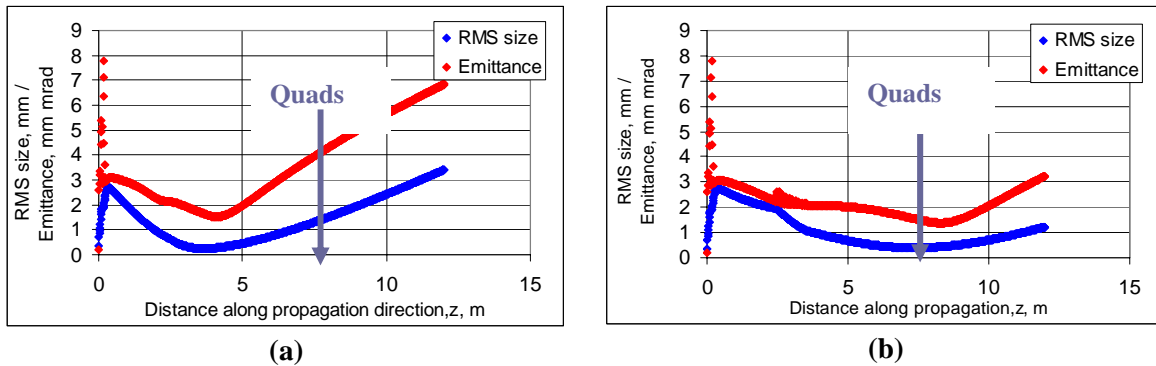
Fig. 9. Emittance and rms beam size evolution for beam focussed at (a) EMSY1 (B = -0.2353 T) and (b) High2.Scr1. (B = -0.2252 T)

5.2.2 Quadrupole scan
ASTRA simulations of a single quadrupole scan for rms beam size without and with space charge calculation were performed and the results are presented in Fig. 10(a) and 10(b), respectively. The fitting values from these simulations were used in the transformation matrix calculation (described in section 3) and the results are shown in Table 4, compared to the results extracted from ASTRA.
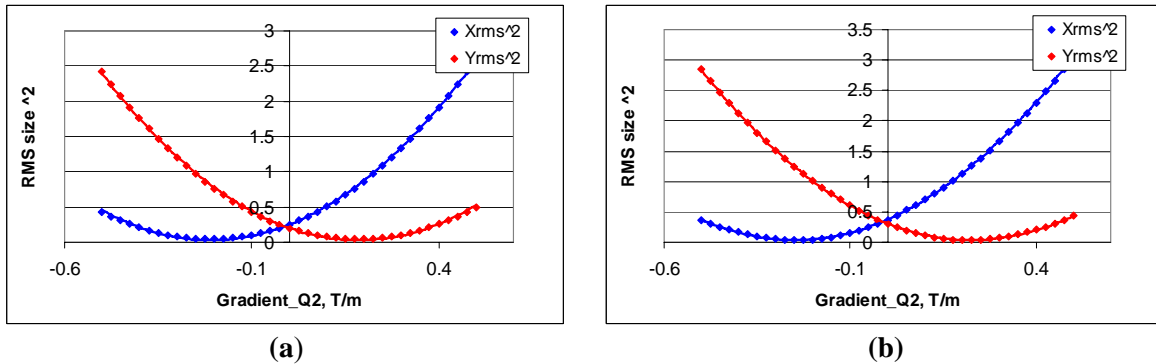
Fig. 10. ASTRA simulations of quadrupole scans without (a) and with (b) space charge.

10

	Without space charge		With space charge	
	ASTRA	Matrix Algorithm	ASTRA	Matrix Algorithm
$\varepsilon_{x \ (mm \ mrad)}$	1.542	1.404	1.540	1.609
$\varepsilon_{y \ (mm \ mrad)}$	1.538	1.396	1.538	1.605
$\varepsilon_{\ (mm \ mrad)}$	1.540	1.400	1.539	1.607

Table 4. Comparison of calculated emittance with transformation matrix algorithm and those given by ASTRA.

In Fig. 10, one can see that the minimum rms beam size is smaller in the simulations than in the experimental values, probably due to the systematic error in measurement. In the experiment, the minimum rms size was 0.32 mm corresponding to a quadrupole field gradient of -0.20 T/m while the minimum rms size in the simulations was 0.215 mm at a quadrupole field gradient of 0.22 T/m.

When space-charge is not included in the simulation, the fitting algorithm (which also does not consider space-charge effects) underestimates the emittance. However, when space charge is included in the simulation and the same fitting algorithm is used, the algorithm overestimates the emittance. The difference in values between when space charge is included and when it is not, obtained in each case is around 15 %. To determine the effects of space charge on the fitting precision it is necessary to refine the fitting algorithm further to obtain more accurate results.

In addition, the ASTRA simulation included a cylindrical space-charge algorithm. For the quadrupole scan it is necessary to use a 3-dimensional space-charge algorithm since for highly focussed beams in one direction, the cylindrical algorithm will not give accurate results due to the difference in particle density in the perpendicular planes. The 3-dimensional algorithm was not used since it is more time-consuming, but it should be investigated further.
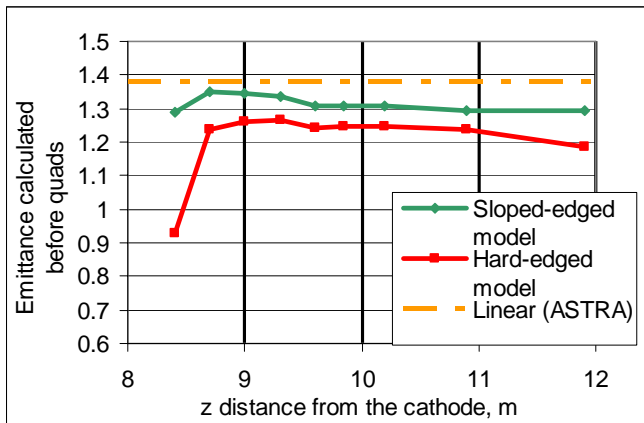
(a) Emittances calculated for different values of drift space between the quadrupoles and the observation point.

(b) Schematic depiction of the field distribution of the hard-edged model

(c) Schematic depiction of the field distribution of the sloped-edged model
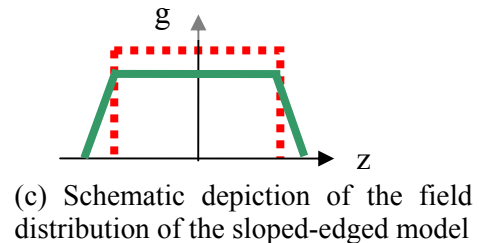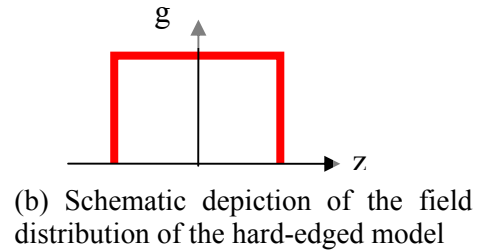
Fig. 11. Comparison of emittance values calculated using the basic hard-edged model, the sloped edged model, and the emittance value predicted by ASTRA.

The length of drift space after the quadrupoles was varied to investigate the dependency of the calculated emittance value on the drift space. At no distance did the calculated value match the value given by the

simulation program. This is because the algorithm used for fitting the data follows the hard-edge approximation as shown in Fig. 11(b). The matrix product should be modified to include fringe field effects. The model was altered to one similar to that shown in Fig. 11(c). This was chosen such that the rms sizes and beam divergence were matched to the corresponding values given by the ASTRA simulation.

The sloped edged model improved the fitted values to some degree as illustrated in Fig. 11(a). However, the model still needs to be improved further. The most promising way to do this is to approximate the real smooth field distribution to a trapezoid such that $\int gdz$ is the same for both cases [6]. The trapezoidal approximation is defined by a fringe field extending over a length equal to the bore radius R. This profile can then be included in the matrix algorithm by decomposing the edges of the field profile into segments of hard edge quadrupoles, each with different field strengths.
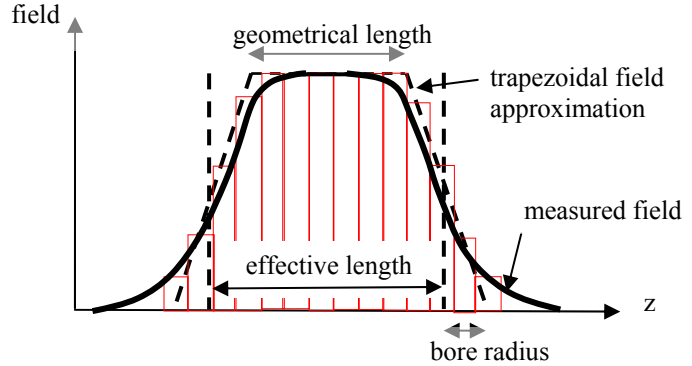
Fig. 12. Trapezoidal approximation to a real smooth field distribution.

This approximation should be possible to implement for the algorithm to fit the experimental data, since the magnetic field is known [9]. However, it is difficult to verify, since ASTRA uses a different algorithm which is not stated in the literature. Without this knowledge, it is impossible to match the fitting algorithm to the algorithm used in ASTRA simulations.

6. SUMMARY AND OUTLOOK

The quadscan method for application at PITZ was investigated. Preliminary measurements at the quadrupole triplet were performed for single- and multi- quadrupole scans. The measurements were compared with ASTRA simulations. The simulations are useful for the development of a protocol for this technique at PITZ. However, there are still a number of improvements to be made to the method before this technique can be implemented as a reliable and accurate measurement procedure. Further work should include the following:

1) Since the solenoid current affects the emittance, a screen at or near the entrance to the quadrupole magnets should be inserted if possible. This would enable the minimum emittance to be measured, rather than some larger value.

2) The step function, or hard-edged model, used to describe the field in the quadrupoles does not give sufficiently accurate results. A trapezoidal approximation to the field in the quadrupoles should be implemented in the fitting algorithm by including a number of smaller matrices of different field strength along the edges of the field.

3) It is necessary to check the influence of the beam alignment through the quads on the emittance measurements.

4) It should be verified theoretically whether it is possible to fit data on the slope of the rms size surface shown in Fig. 6.

12

7. REFERENCES

[1] "Flash – the Free Electron Laser in Hamburg", http://flash/desy.de, accessed 10/09/2007
[2] Miltchev, V., "Investigations on the transverse phase space at a photo injector for minimized emittance", PhD thesis, Humboldt Universitat zu Berlin, 02/03/2006
[3] S. Khodyachykh *et al.,* "New beam diagnostic developments at the photo-injector test facility PITZ", Proceedings of PAC07, Albuquerque, New Mexico, USA
[4] Gierman, S. M., "Streak Camera Enhanced Quadrupole Scan Technique for Characterizing the Temporal Dependence of the Trace Space Distribution of a Photoinjector Electron Beam", PhD thesis, University of California, San Diego, 1999
[5] Rossbach, J., and Schmueser, P., "Basic course on accelerator optics"
[6] Wiedemann, H., "Particle Acelerator Physics", Springer, 3rd Edition, 2007
[7] Staykov, L., "Commissioning of a New Emittance Measurement System at PITZ", FEL 2006, Berlin, Germany
[8] http://www.desy.de/~mpyflo/, accessed 10/09/2007
[9] Bohnet, I, "Magnetic Field Measurements on the PITZ Quadrupole Triplet", 2002

8. ACKNOWLEDGEMENTS